SLC4A1 MUTATIONS THAT CAUSE DISTAL RENAL TUBULAR ACIDOSIS ALTER CYTOPLASMIC PH AND CELLULAR AUTOPHAGY

Grace Essuman[1], Midhat Rizvi[1], Ensaf Almomani[6], Shahid A. K M. Ullah[1,5], Sarder M. A. Hasib[3], Forough Chelangarimiyandoab[1], Priyanka Mungara[1], Manfred J. Schmitt[3], Marguerite Hureaux[2], Rosa Vargas-Poussou[2], Nicolas Touret[4] & Emmanuelle Cordat[1*]

[1]Department of Physiology, University of Alberta, Edmonton, AB, Canada.

[2]Department of Genetics, Georges Pompidou European Hospital, Paris, France.

[3]Department of Molecular and Cell Biology, Department of Biosciences (FR 8.3) and Center of Human and Molecular Biology (ZHMB), Saarland University, Saarbrücken, Germany.

[4]Department of Biochemistry, University of Alberta, Edmonton, AB, Canada.

[5]Department of Medicine, University of Alberta, Edmonton, AB, Canada.

[6]Department of Basic Medical Sciences, Faculty of Medicine, Al-Balqa Applied University, Al-Salt, Jordan

[*] To whom correspondence should be addressed: Department of Physiology, Membrane Protein Disease Research Group, Room 7-34, Medical Sciences Building, University of Alberta, Edmonton, Alberta, T6G 2H7, Canada, Tel: 780-492-8892, Fax: 780-492-8915, e-mail: cordat@ualberta.ca

Key words: kidney, transporters, membrane protein, acidosis, epithelium, trafficking, distal renal tubular acidosis, autophagy, lysosome.

Abstract

Distal renal tubular acidosis (dRTA) is a disorder characterized by the inability of the collecting duct system to secrete acids during metabolic acidosis. The pathophysiology of dominant or recessive *SLC4A1* variant related dRTA has been linked with the mis trafficking defect of mutant kAE1 protein. However, *in vivo* studies in kAE1 R607H dRTA mice and humans have revealed a complex pathophysiology implicating a loss of kAE1-expressing intercalated cells and intracellular relocation of the H^+-ATPase in the remaining type-A intercalated cells. These cells also displayed accumulation of ubiquitin and p62 autophagy markers. The highly active transport properties of collecting duct cells require the maintenance of cellular energy and homeostasis, a process dependent on intracellular pH. Therefore, we hypothesized that the expression of dRTA variants affect intracellular pH and autophagy pathways. In this study, we report the characterization of newly identified dRTA variants and provide evidence of abnormal autophagy and degradative pathways in mouse inner medullary collecting duct cells and kidneys from mice expressing kAE1 R607H dRTA mutant protein. We show that reduced transport activity of the kAE1 variants correlated with increased cytosolic pH, reduced ATP synthesis, attenuated downstream autophagic pathways pertaining to the fusion of autophagosomes and lysosomes and/or lysosomal degradative activity. Our study elucidated a close relationship between the expression of defective kAE1 proteins, reduced mitochondrial activity and decreased autophagy and protein degradative flux.

Introduction

Distal renal tubular acidosis (dRTA) is a disorder characterized by the inability of the collecting duct system to secrete acids during metabolic acidosis[1]. In addition to hyperchloremic metabolic acidosis, patients with this disease can present with hypokalemia, kidney stones, urinary sodium waste and difficulty to thrive. Expression of pathogenic variants in the *ATP6V0A4*, *ATP6V1B1*, *FOXI1*, *WDR72* and *SLC4A1* genes are the usual genetic aetiologies[2–4]. The *SLC4A1* gene encodes the anion exchanger 1 (AE1) protein, which is an electroneutral chloride/bicarbonate exchanger[5]. It exists in two forms: a 911 amino acid erythroid isoform known to interact with erythroid cytoskeletal proteins and participate in red cell respiration and integrity, and a 65 amino acid (NH_2-terminal) truncated isoform primarily found in the basolateral membrane of renal type A intercalated cells (A-IC)[6,7] and podocytes[8]. This isoform participates in bicarbonate reabsorption and through its physical and functional interaction with the cytosolic carbonic anhydrase II and apical H^+-ATPase, it supports apical proton export and urine acidification[9].

Pathogenic variants in the *SLC4A1* gene can result in either red cell defects (such as Southeast Asian ovalocytosis[10,11] and hereditary spherocytosis[12]), renal cell defects (dRTA[10]) or both in patients with homozygous (Band 3 Coimbra and Band 3 Courcouronnes[13,14]) or compound heterozygous variants[15,16]. Renal *SLC4A1* disease-causing variants have only been found in the transmembrane domain - where it could impact protein structure and its transport function- or in the short carboxyl domain – where it possibly affects protein-protein interactions. The pathophysiology of dominant or recessive *SLC4A1* related dRTA (hereafter named dRTA) has originally been linked with the mis-trafficking defect of mutant kAE1 protein[10,17]. However, recent *in vivo* studies in mice and humans have revealed a complex pathophysiology where a loss of kAE1-expressing intercalated cells, the intracellular

relocation of the H^+-ATPase and accumulation of autophagy marker p62 and ubiquitin-positive material in the remaining type-A intercalated cells was suggested to be the principal cause of the disease[18].

The highly active transport properties of collecting duct cells require the maintenance of cellular energy and homeostasis. The autophagy-mediated turnover of damaged organelles is necessary for protecting collecting duct cells as in most renal cells[19]. The chloride/bicarbonate exchange function of kAE1 in A-ICs confers a pivotal role in pH homeostasis and thus is a major contributor to cellular homeostasis. kAE1 protein interacts with several proteins such as integrin-like kinase (ILK), adaptor-related protein complex 1, 3 & 4 (AP-1, AP-3 & AP-4 mu1A), transmembrane protein 139 (TMEM139), kinesin family member 3B (KIF3B), and clathrin among others[7,20–22] that support protein stability and trafficking. It also interacts with homeostatic proteins including the glycolytic enzyme glyceraldehyde-3-phosphate dehydrogenase (GAPDH)[23] and the antioxidant enzyme peroxiredoxin 6 (PRDX 6)[24], which play major roles in cellular energy metabolism and oxidative stress response, respectively.

In this study, we report the characterization of newly identified dRTA variations and provide evidence of abnormal autophagy and degradative pathways in cells and kidneys from mice expressing dRTA mutant kAE1 proteins.

Concise Methods

Ethics Approval

This study was conducted in accordance with all national and institutional animal care guidelines and approved by the University of Alberta's Animal Care and Use Committee (AUP #1277).

Newly identified *SLC4A1* variations from dRTA patients

The patient carrying the R295H mutation was a boy carrying the variation in the homozygous state, whose genetic diagnosis was made at the age of 5, following growth retardation of -2 SD for both weight and height, with bicarbonate at 18 mmol/L, potassium at 2.8 mmol/L, chloridemia at 94 mmol/L, calcemia at 2.55 mmol/L, and a urinary pH of 7.5. He also had a history of a pyeloureteral junction syndrome that was surgically managed at the age of 3. The R295H dRTA variation is a nonsense homozygous substitution characterized by a replacement of guanine (G) on position 884 by adenine (A) in the coding sequence. It has an allelic frequency of 0.14 % in the European population.

For the Y413H variant, the patient was a female diagnosed at 1 month old, with an urinary pH of 7.5, evidence of nephrocalcinosis and failure to thrive. The S525F variant has been previously reported[25], but in brief, the patient was a 13 year old female with plasma pH of 7.25, plasma bicarbonate at 15.3 mmol/L who also presented with polyurethral junction syndrome, nephrocalcinosis and nephrolithiasis since childhood. The Y413H and S525F dRTA variations are nonsense heterozygous substitutions characterized by a replacement of thymine (T) at position 1237 by cytosine (C) and a replacement of cytosine (C) at position 1574 by thymine (T), respectively. The R589H dRTA variation has been previously described[18]. No follow up data were available for all patients.

Mice

Transgenic mice carrying the R607H knockin (KI) mutation (murine equivalent to human R589H mutation) were previously described[18]. Homozygous mice used throughout the study display incomplete dRTA with alkaline urine without metabolic acidosis at baseline as previously reported[18]. Homozygous mice or wild-type (WT) littermates were fed a standard rodent chow (Picolab® Rodent Diet 20 # 5053, LabDiet, ST. Louis, MO, USA) or for Figure 5 (H-K), a salt-depleted diet with acid challenge as previously reported[26] with adequate and constant water supply, and maintained on a 12-hour light and dark cycle throughout their lifespan.

Statistical analysis

All the experiments were independently repeated a minimum of three times. Experimental results were analyzed using the GraphPad Prism software and are summarized as mean ± SEM. All statistical comparisons were made using unpaired Student's t test or one/two-way ANOVA followed by a post-hoc test as indicated in figure legends. A P-value less than 0.05 was considered statistically significant. All datasets were assessed for normality, and outliers identified by Prism were excluded.

Detailed Material and Methods are listed in the Supplementary Material

Results

The dRTA kAE1 variants traffic to the basolateral membrane but have reduced transport activity in mIMCD3 cells.

We first characterized three newly identified dRTA mutations and compared them with kAE1 WT or previously characterized kAE1 R589H mutant. **Figure 1A** depicts the alpha fold predicted structure of kAE1 showing amino acids mutated in each kAE1 mutant. kAE1 R295H is a recessively inherited substitution in the N-terminal cytosolic domain of the protein. kAE1 Y413H is a dominantly inherited substitution in transmembrane domain (TM) 1 of the core domain. In the gate domain, S525F and R589H substitutions occur in TM 5 and TM 6, respectively. We generated the newly identified dRTA variant cDNAs and expressed them or kAE1 WT in mIMCD3 cells to assess protein abundance (**Figure 1B**), localization (**Figure 1C, D**), transport activity (**Figure 1E**) and lifespan (**Figure 1F**). As seen on **Figure 1B,** both kAE1 R295H and S525F variants display 2 typical bands similar to kAE1 WT. The top band encompasses kAE1 proteins carrying a complex oligosaccharide that have reached the Golgi and beyond, while the bottom band corresponds to high mannose-carrying kAE1 proteins located in the endoplasmic reticulum. However, kAE1 Y413H mutant bands intensity was overall weaker than WT and displayed a predominant single band aligned with high mannose-carrying kAE1 proteins. These results indicate that the 3 newly described dRTA mutants are expressed in mIMCD3 cells. We next localized these mutants by immunofluorescence in mIMCD3 cells. While kAE1 WT is targeted to the plasma membrane, the kAE1 R295H, Y413H and S525F variants partially colocalize with endoplasmic reticulum marker calnexin (**Figure 1C**). Yet, both kAE1 WT and mutants appropriately co-localized with basolateral membrane marker beta-catenin in polarized mIMCD3 cells **(Figure 1D)**. However, when the transport function was assayed on confluent

cells, both kAE1 Y413H and S525F had significantly lower transport activity than WT (**Figure 1E)** and were not significantly different from un-induced WT-Dox cells (not shown on the graph). Finally, we observed that degradation of the kAE1 Y413H mutant begins 6 hours post-synthesis while kAE1 WT abundance remained stable for 24 hours (**Figure 1F**). Given this premature degradation, we did not perform further assays on cells expressing the Y413H protein. Overall, these results indicate that except for kAE1 Y413H mutant, the other mutants are expressed and traffic to the basolateral membrane of polarized mIMCD3 cells, similar to the previously published kAE1 R589H mutant.

Expression of the kAE1 R295H, S525F and R589H dRTA mutants alter autophagy processes in mIMCD3 cells and whole kidney lysates.

In mice expressing kAE1 R607H, a striking reduction in type-A intercalated cells was noted and in the remaining cells, autophagy marker p62 and ubiquitin accumulated in these abnormally enlarged cells[18]. We therefore investigated the autophagy machinery in dRTA mutant mIMCD3 cells and in R607H knockin (KI) mice. We first examined the ratio of autophagosome marker LC3BII protein relative to the total intensities of LC3BI and LC3BII as well as p62 levels. These experiments were performed at steady state, upon autophagy induction by starvation, or after autophagy inhibition by Bafilomycin (Baf) A1 **(Figure 2A-C)**. **Figure 2A – I** show a consistent increase in the ratio of LC3B II to total LC3B (I + II) in the mutant cells at steady state (**panel D**), with starvation (**panel F**) and with Baf A1 (**panel H**) except for the kAE1 R295H mutant which was not significantly different from WT at steady state only. This suggests an altered autophagy process in the mutant cells, in agreement with preliminary findings from Mumtaz and colleagues[18]. There was no significant difference in p62 abundance in mutant cells compared to WT at steady state and with starvation (**Figure 2E-G**). However, with Baf A1, R589H mutant cells had significantly lower p62 abundance

compared to WT (**Figure 2I**). To confirm these findings, we next assessed the abundance of these markers in whole kidney lysates from the kAE1 R607H KI mice. We observed that the total LC3B abundance was significantly higher in homozygous KI mice (KI/KI) compared to WT, with no difference in p62 (**Figure 2J-L)**. Overall, these results suggest an abnormal autophagy in mutant mIMCD3 cells and in kidneys of R607H KI mice.

dRTA kAE1 mutant expressing cells have more alkaline intracellular pH than WT and altered autophagy flux.

Given these preliminary findings of abnormal autophagy in the dRTA mutant cells, we next assessed the efficiency of the autophagy machinery in WT or dRTA mutant-expressing cells using the eGFP-RFP-LC3 construct (**Figure 3A**). The green fluorescent protein fused to LC3 is quenched in the acidic environment of the autolysosome, while both eGFP and RFP fluoresce in vesicles in the neutral lumen of the autophagosome[27,28]. Focusing on cells expressing either kAE1 S525F or R589H, we quantified the number of eGFP+ (green), RFP+ (red) and double eGFP+/RFP+ (yellow) vesicles in the kAE1 mutant or WT transfected live cells (**Figure 3B-D**). kAE1 S525F mutant cells have significantly more autophagosomes (yellow) than WT counterparts (**Figure 3B),** and both kAE1 S525F and R589H have significantly more autolysosomes (red) than WT (**Figure 3C). Figure 3D** shows that both mutants, particularly the kAE1 S525F mutant cells had significantly more autophagosomes than autolysosomes. This finding suggests an upregulation of autophagy and inhibition in the downstream steps of autophagy that involves the fusion of the autophagosome with the lysosome[29]. As autolysosomes require luminal v-H^+-ATPase -dependent acidification to efficiently clear cell debris [30] and as kAE1 is a base transporter whose function is linked to the v-H^+-ATPase, we next wondered whether the steady-state cytosolic pH of mIMCD3 cells expressing kAE1 WT or mutant was different. Using BCECF-AM, we observed that the

steady state intracellular pH (pHi) of kAE1 mutant cells was more alkaline than WT cells (except for kAE1 R295H cell pHi which has a similar trend but is not significantly different from WT) (**Figure 3E**), in agreement with transport activity (**Figure 1F**). Given the lack of difference in phenotype between the kAE1 R295H and kAE1 WT mIMCD3 cells, we focused the subsequent experiments on kAE1 S525F and R589H mutant cells. As a higher intracellular pH could contribute to alterations in the autophagy machinery[31], we chemically acidified the cytosolic pH of cells expressing kAE1 mutant or WT and examined autophagy and lysosomal markers (**Figure 3 F-H**). We first determined that incubation of mIMCD3 cells in 0.033 μM nigericin for 2 hours acidified cytosolic pH to 6.9 without causing cell death (**Supplementary Figure 1**). We observed that chemically reducing pHi to 6.9 in mutant expressing cells reduced the ratio of LC3B II to total LC3B (**Figure 3I)** and the abundance of lysosomal-associated membrane protein 1 (LAMP1) in R589H cells (**Figure 3 J)** to levels similar to WT cells at steady state. These findings suggest that abnormal autophagy in the mutant cells may be caused by their alkaline pHi, resulting from a reduced anion exchange activity of the mutant kAE1 protein.

mIMCD3 cells expressing dRTA kAE1 mutants and R607H KI kidney tissues have abnormal lysosome number and size.

The accumulation of autophagosomes and autolysosomes as seen above may suggest one or a combination of the following: an inability of autophagosomes to fuse with lysosomes and/ or a defect in lysosomal degradative activity in the mutant cells[19,32]. We first examined the lysosomal degradative activity by assessing lysosomal protease Cathepsin B activity using Magic Red staining (**Figure 4A-B).** In agreement with increased RFP+ vesicles (**Figure 3D**), the kAE1 S525F mutant cells had a significantly higher number of Magic Red positive vesicles than WT whereas the kAE1 R589H mutant cells had significantly larger Magic Red

positive vesicles, suggesting an accumulation of undigested material[33]. To validate this finding, we performed immunostaining and quantified LAMP1 positive staining in ß1 ATPase positive cells (a marker of ICs) in WT and R607H KI mouse kidney sections. The KI mice showed significantly more and larger LAMP1 positive vesicles compared to WT mice in both cortex and medulla (**Figure 4 C-F**). We probed further into the lysosomal activity by quantifying lysosomal protease Cathepsin D (immature, intermediate and mature) protein abundance by immunoblot in isolated primary murine A-ICs. Although the abundance of immature and intermediate cathepsin D did not differ between genotypes, the KI mice showed a significantly decreased abundance of mature cathepsin D (**Supplementary Figure 2**). Thus, in line with *in vitro* findings, A-IC from homozygous R607H KI mice display relatively more and larger lysosomes with reduced active protease abundance than WT littermates, suggesting a lysosomal defect in the dRTA kAE1 mutant cells.

dRTA kAE1 mutant cells have lower ATP production rate and abnormal mitochondrial content.

Lysosomal degradation is highly dependent on a low luminal pH generated in part by the vacuolar-type H^+-ATPase[34] whose activity depends on ATP hydrolysis. We therefore analysed the ATP production rate in mIMCD3 cells, specifically glycolysis and oxidative phosphorylation. We measured the oxygen consumption rate (OCR) (**Figure 5A**) and extracellular acidification rate (ECAR) in empty vector transfected, kAE1 WT or mutant cells (**Figure 5B**). Both kAE1 S525F and R589H mutant cells had a lower ATP production rate compared to WT (**Figure 5C**). More specifically, the R589H mutant cells had a lower mitochondrial ATP production rate (**Figure 5D**) whereas the kAE1 S525F mutant cells exhibited a lower glycolytic ATP production rate (**Figure 5E**). With the mitochondria being the major ATP-producing organelles[35], we assessed mitochondrial content by

immunostaining of translocase of the outer membrane 20 (TOM20) both *in vitro* and *in vivo.* Both kAE1 S525F and R589H mutant cells have higher mitochondrial content compared to WT as determined by total overall intensity of TOM20 positive puncta (**Figure 5F&G**). In line with this result, although a decreased fluorescence intensity was observed in the cortex, there was a significantly higher TOM20 fluorescence intensity in medullary kidneys of homozygous R607H KI mutant mice compared to WT littermates (**Figure 5H-K**).

Discussion

In this study, we characterized three newly identified dRTA-causing kAE1 variations. Combining *in vivo* and *in vitro* studies, we demonstrated that reduced transport activity of the kAE1 mutants correlated with increased cytosolic pH, reduced ATP synthesis, attenuated downstream autophagic pathways and lysosomal dysfunction, pertaining to the fusion of autophagosomes and lysosomes and/ or lysosomal degradative activity.

In line with previous observations[18], the kAE1 R295H, Y413H and S525F mutants were intracellularly retained in non-polarised mIMCD3 cells but properly localized to the basolateral membrane after polarization. When expressed in Madin-Darby canine kidney (MDCK) cells, other dRTA-causing kAE1 mutants such as dRTA R602H, G701D, V488M, deltaV850 variants also exhibited a plasma membrane trafficking defect[10,36,37]. In contrast, the kAE1 R589H mutant was correctly targeted to the plasma membrane[18]. Functionally, cells expressing the Y413H and S525F mutants exhibit about 40 % reduction in chloride/bicarbonate exchange activity compared to kAE1 WT, similar to the previously characterized recessive G701D mutant but unlike the R295H mutant[38]. Therefore, the mechanism causing dRTA remains unclear in the case of the newly identified R295H variant. These findings add to the growing list of *SLC4A1* gene variations causing dRTA.

We next investigated the roots of the altered autophagy briefly reported in R607H KI mice[18] using mIMCD3 cells and whole kidney lysates. In kidneys of the KI mice, a decrease in A-IC, accumulation of p62 and ubiquitin and enlarged remaining A-ICs, prompted us to investigate autophagy pathways in dRTA mutant cells and in homozygous R607H KI mice[18,38]. During the autophagy process, LC3B I (a marker for autophagosomes) is converted to lipidated LC3B II[39] and p62 aggregates to facilitate the degradation of ubiquitinated proteins within the autophagosome complex[40]. In mIMCD3 cells, LC3B lipidation was increased in the kAE1 R295H, S525F and R589H mutant cells compared to WT, an increase

that persisted with both Baf A1 treatment and starvation. Although opposite effects were expected under inhibition or induction of autophagy, such similar effect has been previously described. In the proximal tubule of obese mice, LC3B accumulation indicating a stagnated autophagy flux, was observed with both chloroquine treatment and 24 hour starvation[41]. Similarly, in NRK-52E cells, a disruption of the autophagy machinery by LC3B II accumulation in high cadmium-stressed cells occurred under either Baf A1 or rapamycin (an autophagy inducer) treatment[42]. Although LC3B II is elevated during both increased autophagy flux and disrupted autophagy, we did not observe significant accumulation of p62 in mIMCD3 cells expressing dRTA mutants. p62 is specifically a marker of autophagy-mediated protein clearance[43–45]. Therefore, p62 accumulation in R607H KI mouse kidney sections strongly suggests a compromised autophagy-mediated clearance while the increased LC3B lipidation without significant changes in p62 in mIMCD3 cells points towards either an increased autophagic flux and/or a disrupted autophagy.

To obtain a clearer picture of the precise autophagic pathway altered in the dRTA mutants, we probed further into the different stages of autophagy and autophagy flux. We noted an accumulation of autophagosomes and autolysosomes in the S525F and R589H mutant cells. This was recapitulated in the R607H KI mice which showed significantly more and bigger LAMP 1 positive vesicles in both kidney cortex and medulla, suggesting a blockage in autophagy flux in both dRTA mutant cells and KI mice. Such blockage has been implicated in the pathophysiology of several diseases. In lysosomal storage disease, lysosome accumulation in proximal tubule cells is a key component in the pathways mediating epithelial dysfunction[19]. In this study, restoring autophagy flux attenuated disease progression. Another study in SK-N-SH, RT4-D6P2T and HeLa cells implicated autophagosome and lysosome accumulation in cellular toxicity associated with neurodegenerative diseases[32]. In agreement with altered lysosomal function, we also noted a

greater abundance and size of active cathepsin B lysosomal protease vesicles in mIMCD3 cells. Increased cathepsin B activity affects lysosomal biogenesis, autophagy initiation and cellular homeostasis[46]. In the renal context, cathepsin B knockout mice demonstrated a higher resistance and quicker recovery from glomerular damage[47], suggesting that cathepsin B accumulation may be detrimental to the cells. Increased cathepsin B abundance in the dRTA mutant cells also correlates with the accumulation of lysosomes. Overall, these findings suggest that the pathogenesis of dRTA in our models involves an inhibition of autophagy flux at the downstream steps involving autophagosome-lysosome fusion and lysosomal protein clearance [29,33,48,49].

The question remained as to how these dRTA variants altered autophagy. The *SLC4A1-3* gene family that includes AE1 are regulators of intracellular pH in different cell types[50–52]. The reduced anion exchange activity in mIMCD3 cells expressing the R589H and S525F variants expectedly correlated with an increased pHi compared to WT counterparts. We wondered whether this was the mechanism explaining blockade in autophagy flux since pHi variations impact autophagy[31,34,53–55]. Previous studies reported more perinuclear localization of lysosomes and autophagosome-lysosome fusion in cells with an increased pHi[53,54]. Although not examined in our study, an increase in intracellular pH due to starvation decreased the levels of lysosomal kinesin superfamily member KIF2 and ADP-ribosylation factor-like 8B (ARL8), which are responsible for redistributing lysosomes to the cell periphery. This reduction subsequently inhibited mTORC1, resulting in increased autophagosome synthesis and autophagosome-lysosome fusion[53].

While an alkaline cytosolic pH partially explains the impairment in autophagy flux, a close relationship also exists between intracellular pH and cellular energy dynamics and metabolic stress, all of which are key regulators of autophagy[56]. Therefore, it was plausible that kAE1 variant-induced autophagy dysregulation occurs through a signalling pathway akin

to that of energy deprivation-induced autophagy. This hypothesis is supported by our findings of reduced ATP production rate in dRTA kAE1 S525F and R589H mutant cells compared to kAE1 WT cells. We also found that both kAE1 S525F and R589H mutant cells have higher mitochondrial content compared to kAE1 WT cells. The increased mitochondrial content coupled with low ATP point towards improper mitochondrial function in dRTA variant cells. Low ATP levels as seen in dRTA mutant cells may impair autophagy as was shown in human RPE cells[57]. ATP reduction in RPE cells led to complex mitochondrial changes such as structural disorganization, enzyme activity decline, and oxidative damage to mitochondrial components and DNA[57]. Similarly, in pancreatic islet cells, an alkaline pHi led to increased uptake of phosphate by mitochondria, accelerating the production of superoxide, promoting mitochondrial permeability transition, and inducing translational attenuation due to endoplasmic reticulum stress, ultimately impairing insulin secretion[58]. Overall, our data support that expression of the kAE1 variants increases pHi which alters mitochondrial function and leads to reduced cellular energy levels that eventually attenuates energy-dependent autophagic pathways including autophagosome-lysosome fusion and lysosomal protein clearance.

In light of these observations, we postulated that correcting the alkaline pHi of dRTA mutant-expressing mIMCD3 cells will alleviate this blockage in autophagy flux. We observed that a chemically engineered pHi of 6.9[59] reduced LC3B II accumulation and LAMP1 abundance in mIMCD3 mutant cells to expression levels similar to that of WT cells at baseline. This suggests that a chemically reduced pHi facilitated protein clearance in the two dRTA mutant cells[31,53] as noted in other studies. In one such study, treatment of SH-SY5Y cells with FCCP and nigericin also acidified intracellular pH and triggered autophagy and mitophagy[31]. Similarly, acid loading in proximal tubular cells under chronic metabolic acidosis showed increased autophagic flux and mitophagy[60]. These findings are in line with

our results and establish a link between altered autophagy flux and the alkaline pHi of dRTA variant cells.

In conclusion, our study established a strong relationship between the expression of defective kAE1 proteins, reduced mitochondrial activity, decreased autophagy and impaired protein degradative flux. Whether this abnormal degradative pathway explains the premature loss of A-IC will need to be elucidated in further studies.

Acknowledgements

We thank Kristina MacNaughton, Jared Bouchard, Kiera Smith and Hilmar Strickfaden for excellent technical assistance. Imaging experiments were performed at the University of Alberta Faculty of Medicine & Dentistry Cell Imaging Core, RRID:SCR_019200, which receives financial support from the Faculty of Medicine & Dentistry, the University Hospital Foundation, Striving for Pandemic Preparedness – The Alberta Research Consortium, and Canada Foundation for Innovation (CFI) awards to contributing investigators. Services were provided by the University of Alberta Faculty of Medicine & Dentistry Workshop, RRID:SCR_019181, which receives financial support from the Faculty of Medicine & Dentistry.

Disclosure and competing interests statement

The authors have no competing interest to declare.

Funding

This study was funded by the Canadian Institutes of Health Research (PJT#168871) and the Kidney Foundation of Canada (2020KHRG-666615) to E.C, by a grant from the Deutsche Forschungsgemeinschaft to M.J.S. (IRTG 1830) and the Canadian Institutes of Health Research (PS#165816) to N.T. G.E. received a Graduate Student Engagement Scholarship, a Faculty of Medicine and Dentistry Delnor Scholarship and a Faculty of Medicine and Dentistry 75th Anniversary award. M.R. received a Sir Frederick Banting and Dr. Charles Best Canada Graduate Scholarship-Master's (CGS-M) from the Canadian Institutes of Health Research; Walter H. Johns Graduate Fellowship; a University of Alberta Faculty of Medicine and Dentistry/Alberta Health Services Graduate Student Recruitment Studentship (GSRS) and an Alberta Graduate Excellence Scholarship (AGES). A.K.M.S.U. received an NSERC

CREATE graduate studentship. F.C. was supported by a Discovery Grant to E.C. from the Natural Sciences and Engineering Research Council (RGPIN-2017-06432), and was awarded a Graduate Recruitment scholarship from the University of Alberta. S.M.A.H. received a PhD scholarship from the DAAD (Deutscher Akademischer Austauschdienst).

References

1. Giglio, S., Montini, G., Trepiccione, F., Gambaro, G. & Emma, F. Distal renal tubular acidosis: a systematic approach from diagnosis to treatment. *Journal of Nephrology* **34**, 2073–2083 (2021).
2. Escobar, L. I. *et al.* Mutations in ATP6V1B1 and ATP6V0A4 genes cause recessive distal renal tubular acidosis in Mexican families. *Mol. Genet. Genomic Med.* **4**, 303–311 (2016).
3. Rungroj, N. *et al.* Distal renal tubular acidosis caused by tryptophan-aspartate repeat domain 72 (WDR72) mutations. *Clin. Genet.* **94**, 409–418 (2018).
4. Enerbäck, S. *et al.* Acidosis and Deafness in Patients with Recessive Mutations in FOXI1. *J. Am. Soc. Nephrol.* **29**, 1041–1048 (2018).
5. Toye, A. M., Banting, G. & Tanner, M. J. A. Regions of human kidney anion exchanger 1 (kAE1) required for basolateral targeting of kAE1 in polarized kidney cells: Mis-targeting explains dominant renal tubular acidosis (dRTA). *J. Cell Sci.* **117**, 1399–1410 (2004).
6. Kollert-Jons, A., Wagner, S., Hubner, H., Appelhans, H. & Drenckhahn, D. Anion exchanger 1 in human kidney and oncocytoma differs from erythroid AE1 in its NH2 terminus. *Am J Physiol* **265**, F813–F821 (2023).
7. Nuiplot, N. *et al.* Transmembrane protein 139 (TMEM139) interacts with human kidney isoform of anion exchanger 1 (kAE1). *Biochem. Biophys. Res. Commun.* **463**, 706–711 (2015).
8. Wu, F. *et al.* Anion Exchanger 1 Interacts with Nephrin in Podocytes. *J. Am. Soc. Nephrol.* **21**, 1456–1467 (2010).
9. Cordat, E. & Reithmeier, R. A. F. Structure, function, and trafficking of SLC4 and SLC26 anion transporters. *Curr. Top. Membr.* **73**, 1–67 (2014).

10. Sawasdee, N. *et al.* Trafficking defect of mutant kidney anion exchanger 1 (kAE1) proteins associated with distal renal tubular acidosis and Southeast Asian ovalocytosis. *Biochem. Biophys. Res. Commun.* **350**, 723–730 (2006).

11. Cheung, J. C., Cordat, E. & Reithmeier, R. A. F. Trafficking defects of the Southeast Asian ovalocytosis deletion mutant of anion exchanger 1 membrane proteins. *Biochem. J.* **392**, 425–434 (2005).

12. Tang, X., Guo, X. & Gao, J. A Novel Compound Heterozygous Mutation in SLC4A1 Gene Causing Severe Hereditary Spherocytosis and Distal Renal Tubular Acidosis. *Indian Journal of Pediatrics* **87**, 233–234 (2020).

13. Ribeiro, M. L. *et al.* Severe hereditary spherocytosis and distal renal tubular acidosis associated with the total absence of band 3. *Blood* **96**, 1602–1604 (2000).

14. Toye, A. M. *et al.* Band 3 Courcouronnes (Ser667Phe): A trafficking mutant differentially rescued by wild-type band 3 and glycophorin A. *Blood* **111**, 5380–5389 (2008).

15. Chang, Y. H. *et al.* Compound mutations in human anion exchanger 1 are associated with complete distal renal tubular acidosis and hereditary spherocytosis. *Kidney Int* **76**, 774–783 (2009).

16. Khositseth, S. *et al.* Tropical distal renal tubular acidosis: clinical and epidemiological studies in 78 patients. *QJM* **105**, 861–877 (2012).

17. Cordat, E. Unraveling trafficking of the kidney anion exchanger 1 in polarized MDCK epithelial cells. *Biochem. Cell Biol.* **84**, 949–959 (2006).

18. Mumtaz, R. *et al.* Intercalated Cell Depletion and Vacuolar H+-ATPase Mistargeting in an Ae1 R607H Knockin Model. *J. Am. Soc. Nephrol.* **28**, 1507–1520 (2017).

19. Festa, B. P. *et al.* Impaired autophagy bridges lysosomal storage disease and epithelial dysfunction in the kidney. *Nat. Commun.* **9**, (2018).

20. Keskanokwong, T. *et al.* Interaction of Integrin-linked Kinase with the Kidney Chloride/Bicarbonate Exchanger, kAE1. *J. Biol. Chem.* **282**, 23205–23218 (2007).

21. Duangtum, N. *et al.* Human kidney anion exchanger 1 interacts with kinesin family member 3B (KIF3B). *Biochem. Biophys. Res. Commun.* **413**, 69–74 (2011).

22. Sawasdee, N. *et al.* Human kidney anion exchanger 1 interacts with adaptor-related protein complex 1 μ1A (AP-1 mu1A). *Biochem. Biophys. Res. Commun.* **401**, 85–91 (2010).

23. Su, Y. *et al.* Glyceraldehyde 3-phosphate dehydrogenase is required for band 3 (anion exchanger 1) membrane residency in the mammalian kidney. *Am J Physiol Ren. Physiol* **300**, 157–166 (2011).

24. Sorrell, S. L., Golder, Z. J., Johnstone, D. B. & Karet Frankl, F. E. Renal peroxiredoxin 6 interacts with anion exchanger 1 and plays a novel role in pH homeostasis. *Kidney Int.* **89**, 105–112 (2016).

25. Bertocchio, J. P. *et al.* Red Blood Cell AE1/Band 3 Transports in Dominant Distal Renal Tubular Acidosis Patients. *Kidney Int. Reports* **5**, 348–357 (2020).

26. Mungara, P. *et al.* Urinary Sodium Wasting and Disrupted Collecting Duct Function in Mice with dRTA-Causing SLC4A1 Mutations. *bioRxiv* 2024.08.21.608692 (2024). doi:10.1101/2024.08.21.608692

27. Zhou, C. *et al.* Monitoring autophagic flux by an improved tandem fluorescent-tagged LC3 (mTagRFP-mWasabi-LC3) reveals that high-dose rapamycin impairs autophagic flux in cancer cells. *Autophagy* **8**, 1215–26 (2012).

28. Kimura, S., Noda, T. & Yoshimori, T. Dissection of the Autophagosome Maturation Process by a Novel Reporter Protein, Tandem Fluorescent-Tagged LC3. *Autophagy* **3**, 452–460 (2007).

29. Mizushima, N. A brief history of autophagy from cell biology to physiology and

disease. *Nat. Cell Biol.* **20**, 521–527 (2018).

30. Hu, M., Zhou, N., Cai, W. & Xu, H. Lysosomal solute and water transport. *J. Cell Biol.* **221**, 1–14 (2022).

31. Berezhnov, A. V. *et al.* Intracellular pH Modulates Autophagy and Mitophagy. *J. Biol. Chem.* **291**, 8701–8708 (2016).

32. Button, R. W., Roberts, S. L., Willis, T. L., Oliver Hanemann, C. & Luo, S. Accumulation of autophagosomes confers cytotoxicity. *J. Biol. Chem.* **292**, 13599 (2017).

33. de Araujo, M. E. G., Liebscher, G., Hess, M. W. & Huber, L. A. Lysosomal size matters. *Traffic* **21**, 60–75 (2020).

34. Ratto, E. *et al.* Direct control of lysosomal catabolic activity by mTORC1 through regulation of V-ATPase assembly. *Nat. Commun.* **13**, 1–15 (2022).

35. Jonckheere, A. I., Smeitink, J. A. M. & Rodenburg, R. J. T. Mitochondrial ATP synthase: Architecture, function and pathology. *J. Inherit. Metab. Dis.* **35**, 211–225 (2012).

36. Yang, M. *et al.* Mutations and clinical characteristics of dRTA caused by SLC4A1 mutations: Analysis based on published patients. *Front. Pediatr.* **11**, 1077120 (2023).

37. Deejai, N. *et al.* Impaired trafficking and instability of mutant kidney anion exchanger 1 proteins associated with autosomal recessive distal renal tubular acidosis. *BMC Med. Genomics* **15**, 1–12 (2022).

38. Chu, C. Y. S., King, J. C., Berrini, M., Alexander, R. T. & Cordat, E. Functional Rescue of a Kidney Anion Exchanger 1 Trafficking Mutant in Renal Epithelial Cells. *PLoS One* **8**, (2013).

39. Dhingra, A., Alexander, D., Reyes-Reveles, J., Sharp, R. & Boesze-Battaglia, K. Microtubule-associated protein 1 light chain 3 (LC3) isoforms in RPE and retina. *Adv.*

Exp. Med. Biol. **1074**, 609–616 (2018).

40. Huang, X. *et al.* S-acylation of p62 promotes p62 droplet recruitment into autophagosomes in mammalian autophagy. *Mol. Cell* **83**, 3485-3501.e11 (2023).

41. Yamamoto, T. *et al.* High-fat diet-induced lysosomal dysfunction and impaired autophagic flux contribute to lipotoxicity in the kidney. *J. Am. Soc. Nephrol.* **28**, 1534–1551 (2017).

42. Lee, W. K. *et al.* Initial autophagic protection switches to disruption of autophagic flux by lysosomal instability during cadmium stress accrual in renal NRK-52E cells. *Arch. Toxicol.* **91**, 3225–3245 (2017).

43. Brown, C. N. *et al.* Surgical procedures suppress autophagic flux in the kidney. *Cell Death Dis.* **12**, (2021).

44. Mizushima, N., Ohsumi, Y. & Yoshimori, T. Autophagosome formation in mammalian cells. *Cell Struct. Funct.* **27**, 421–429 (2002).

45. Klionsky, D. J. *et al.* Guidelines for the use and interpretation of assays for monitoring autophagy. *Autophagy* **8**, 445–544 (2012).

46. Liu, F. *et al.* Cathepsin B: The dawn of tumor therapy. *Eur. J. Med. Chem.* **269**, 116329 (2024).

47. Höhne, M. *et al.* Single-nephron proteomes connect morphology and function in proteinuric kidney disease. *Kidney Int.* **93**, 1308–1319 (2018).

48. Ballabio, A. & Gieselmann, V. Lysosomal disorders: From storage to cellular damage. *Biochim. Biophys. Acta - Mol. Cell Res.* **1793**, 684–696 (2009).

49. Eskelinen, E. L. Roles of LAMP-1 and LAMP-2 in lysosome biogenesis and autophagy. *Mol. Aspects Med.* **27**, 495–502 (2006).

50. Thornell, I. M. & Bevensee, M. O. Regulators of Slc4 bicarbonate transporter activity. *Front. Physiol.* **6**, (2015).

51. Zhang, Q. *et al.* The structural basis of the pH-homeostasis mediated by the Cl−/HCO3− exchanger, AE2. *Nat. Commun.* **14**, (2023).

52. Romero, M. F., Chen, A. P., Parker, M. D. & Boron, W. F. The SLC4 family of bicarbonate (HCO3-) transporters. *Mol. Aspects Med.* **34**, 159–182 (2013).

53. Korolchuk, V. I. *et al.* Lysosomal positioning coordinates cellular nutrient responses. *Nat. Cell Biol.* **13**, 453–462 (2011).

54. Heuser, J. Changes in lysosome shape and distribution correlated with changes in cytoplasmic pH. *J. Cell Biol.* **108**, 855–864 (1989).

55. Xu, T., Su, H., Ganapathy, S. & Yuan, Z. M. Modulation of autophagic activity by extracellular pH. *Autophagy* **7**, 1316–1322 (2011).

56. Mizushima, N. & Komatsu, M. Autophagy: Renovation of Cells and Tissues. *Cell* **147**, 728–741 (2011).

57. Schütt, F., Aretz, S., Auffarth, G. U. & Kopitz, J. Moderately reduced ATP levels promote oxidative stress and debilitate autophagic and phagocytic capacities in human RPE cells. *Investig. Ophthalmol. Vis. Sci.* **53**, 5354–5361 (2012).

58. Nguyen, T. T. *et al.* Intracellular alkalinization by phosphate uptake via type III sodium-phosphate cotransporter participates in high-phosphate-induced mitochondrial oxidative stress and defective insulin secretion. *FASEB J.* **30**, 3979–3988 (2016).

59. Lyons, J. C., Kim, G. E. & Song, C. W. Modification of intracellular pH and thermosensitivity. *Radiat. Res.* **129**, 79–87 (1992).

60. Namba, T. *et al.* Autophagic clearance of mitochondria in the kidney copes with metabolic acidosis. *J. Am. Soc. Nephrol.* **25**, 2254–2266 (2014).

Figure Legends

Figure 1. kAE1 R295H, Y413H, S525F and R589H dRTA mutants are either dysfunctional or prematurely degraded. (A) Alpha Fold predicted structure of the kidney isoform of Band 3 anion exchanger 1 (kAE1) with core and gate domains highlighted. The dRTA kAE1 mutation sites are coloured in blue with line extensions detailing specific amino acids mutated. (B) Immunoblot showing kAE1 expression and corresponding actin band of mIMCD kAE1 WT, R295H, Y413H, S525F and R589H cells treated with and without doxycycline for 24 hrs. Mouse anti-HA antibody was used to detect kAE1-HA, top and bottom bands correspond to kAE1 carrying complex and high mannose oligosaccharides, respectively. Immunostaining of kAE1 WT or mutant (red) and calnexin (green) in non-polarized mIMCD3 cells (C), and kAE1 WT or mutant (red) and b-catenin (green) in polarized (D) mIMCD cells. Scale bar = 10 µm. Red = kAE1, Green = ß-Catenin. (E) Rate of intracellular alkalinisation in WT or mutant mIMCD3 cells normalized to WT+ Dox. **** indicates P < 0.0001 using one-way ANOVA followed by a Dunnett's post-hoc test. Error bars correspond to mean ± SEM, n= minimum 4. (F) Immunoblot of cycloheximide (CHX) chase assay with corresponding actin in kAE1 mIMCD WT and Y413H cells showing the degradation of kAE1 Y413H after 3hrs CHX incubation.

Figure 2. Autophagy is upregulated in dRTA kAE1 mutants *in vitro* and *in vivo*. (A-C) Immunoblots of LC3 B and p62 with corresponding actin abundance in kAE1 WT, R295H, S525F and R589H mIMCD3 cells at steady state, under starvation (Starv) or 400 nM Bafilomycin A1 (Baf) treatment. (D-I) Quantification of immunoblots shown in A-C showing the ratio of LC3B II to total LC3B and p62. Error bars correspond to mean ± SEM, n= minimum 3. * P<0.05, ** P<0.01, *** P<0.005, ****P < 0.001 using one-way ANOVA followed by a Tukey's post-hoc test. Immunoblots (J) and quantification (K, L) of LC3B and

p62 abundance in kAE1 R607H KI mouse whole kidney lysates Error bars correspond to mean ± SEM, n= minimum 5. ***P < 0.005 using one-way ANOVA followed by a Tukey's post-hoc test.

Figure 3. dRTA kAE1 mutants have more alkaline steady-state intracellular pH and altered autophagy flux. (A) Immunofluorescence staining of kAE1 in eGFP-RFP-LC3 transfected mIMCD3 cells expressing kAE1. GFP = green, RFP = red, kAE1= cyan. Scale bar = 8 μm. Graphical representation of number of yellow (autophagosomes) (B) and red (autolysosomes) (C) puncta per cell expressing kAE1. Error bars correspond to mean ± SEM, n= minimum 32. ** P<0.01, *** P<0.005, ****P < 0.001 using one-way ANOVA followed by a Tukey's post-hoc test. (D) Grouped graph of the number of yellow (autophagosomes) and red (autolysosomes) puncta per cell expressing kAE1 respectively. Note that the statistical analysis displayed only compared yellow and red groups for simplification. Error bars correspond to mean ± SEM, n= minimum 32. ** P<0.01, ****P < 0.001 using two way ANOVA followed by a Sidak's post-hoc test. (E) Graphical representation of intracellular pH measurement of mIMCD kAE1 WT, R295H, Y413H, S525F and R589H cells. Error bars correspond to mean ± SEM, n = minimum 32. *P<0.05, **P<0.01 using one-way ANOVA followed by a Dunnett's post-hoc test. (F-H) Immunoblot of LC3B, LAMP1 and actin in kAE1 WT, S525F and R589H mIMCD3 cells at steady state and under chemically reduced intracellular pH conditions. Graphical representation of the ratio of LC3B II to total LC3B ratio (I) or LAMP 1 (J) at steady state versus at low pHi in mIMCD3 kAE1 WT, S525F and R589H. Black circles indicate steady state cells and triangles indicate low pHi cells. Error bars correspond to mean ± SEM, n= 3. ** indicates P<0.01 using two-way ANOVA followed by a Sidak's post-hoc test.

Figure 4. dRTA kAE1 mutants have bigger or more lysosomes than WT *in vitro* and *in vivo*. (A) Immunofluorescence images of kAE1 WT, S525F and R589H mIMCD3 cells incubated with Magic Red substrate for 1hr at 37°C in the dark. Green = kAE1, magenta = active lysosomes, blue = nuclei. Scale bar =16 µm. (B) Graphical representation of number and size of active lysosomes per cell. Error bars correspond to mean ± SEM, n= minimum 30. **** P<0.0001 using one-way ANOVA followed by Tukey's post-hoc test. Immunofluorescence images of LAMP 1 and ß1 ATPase in kidney cortex (C) or medulla (E) from kAE1 WT and R607H KI mice. Blue = nuclei, magenta = LAMP 1 (lysosomes), Yellow = ß1 ATPase. Scale bar = 8um. Graphical representation of the number and volume of LAMP1 vesicles in ß1 ATPase positive cells in the kidney cortex (D) or medulla (F) of WT or R607H KI mice. Error bars correspond to mean ± SEM, n= 60. **** P<0.001 using Student's t-test.

Figure 5. dRTA kAE1 mutant cells have lower ATP production rate and abnormal mitochondrial content. (A - B) Oxygen consumption rate (OCR) and Extra Cellular Acidification Rate (ECAR) of empty vector transfected cells, kAE1 WT, S525F or R589H mIMCD3 cells analyzed in a Seahorse XFe96 Extracellular Flux Analyzer with the ATP Rate Assay Test Kit. The empty vector transfected cells provided a control for a potential effect of doxycycline on measurements. (C) Graphical representation of the combination of ATP production rates from mitochondrial respiration (mitoATP) and glycolysis (glycoATP) of kAE1 WT, S525F and R589H mIMCD3 cells measured in real-time following sequential injections of oligomycin and Rotenone +Antimycin A. Error bars correspond to mean ± SEM, n= minimum. * $p < 0.05$, ****$p < 0.0001$ using one-way ANOVA followed by Tukey's post-hoc test. Graphical representations of mitochondrial respiration (D) and glycolytic ATP production (E) in kAE1 WT, S525F and R589H mIMCD3 cells. Error bars correspond to

mean ± SEM, n= minimum 8. **P<0.01, ****p < 0.0001 using one-way ANOVA followed by Tukey's post-hoc test. (F) Immunofluorescence staining of TOM 20 and kAE1 in kAE1 WT, S525F and R589H mIMCD3 cells. Blue = nuclei, Magenta = TOM 20, Green = kAE1. Scale bar = 8 µm. (G) Graphical representation of total TOM 20 fluorescence intensity per cell expressing kAE1. Error bars correspond to mean ± SEM, n= minimum 40. ***p < 0.001, ****p < 0.0001 using one-way ANOVA followed by Tukey's post-hoc test. Immunofluorescence images of TOM 20 and ß1 ATPase in kidney cortex (H) or medulla (I) of kAE1 R607H WT and KI mice exposed to a salt depleted diet with an acid challenge[26]. Blue = nuclei, magenta = TOM 20 (mitochondria), Yellow = ß1 ATPase. Scale bar = 8um. (I) Graphical representation of the total TOM 20 fluorescence intensity in ß1 ATPase positive cells in the cortex (J) or medulla (K) of the kidney. Error bars correspond to mean ± SEM, n= 90. * p < 0.05, ****p < 0.0001 using Student's t-test.

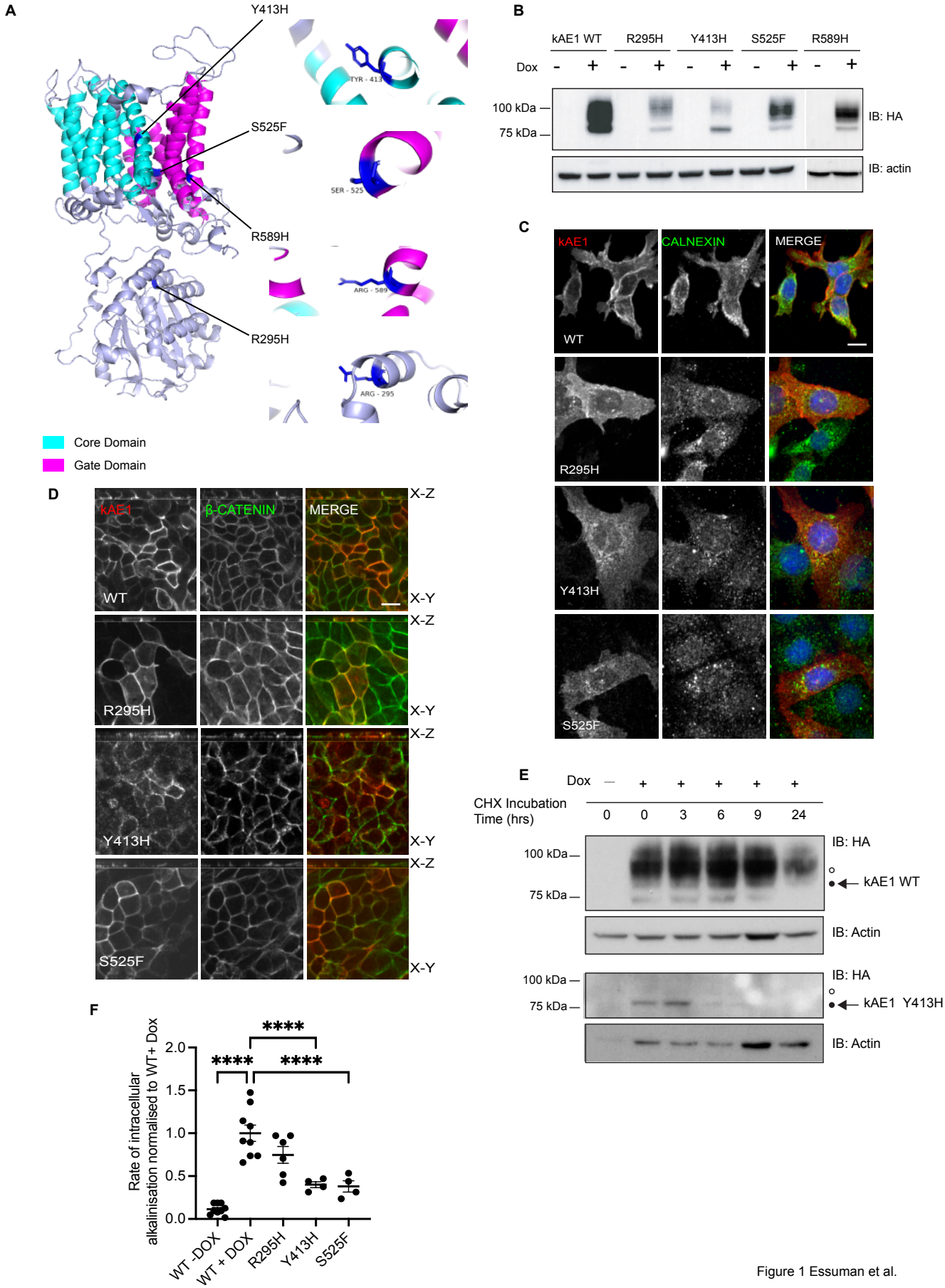

Figure 1 Essuman et al.

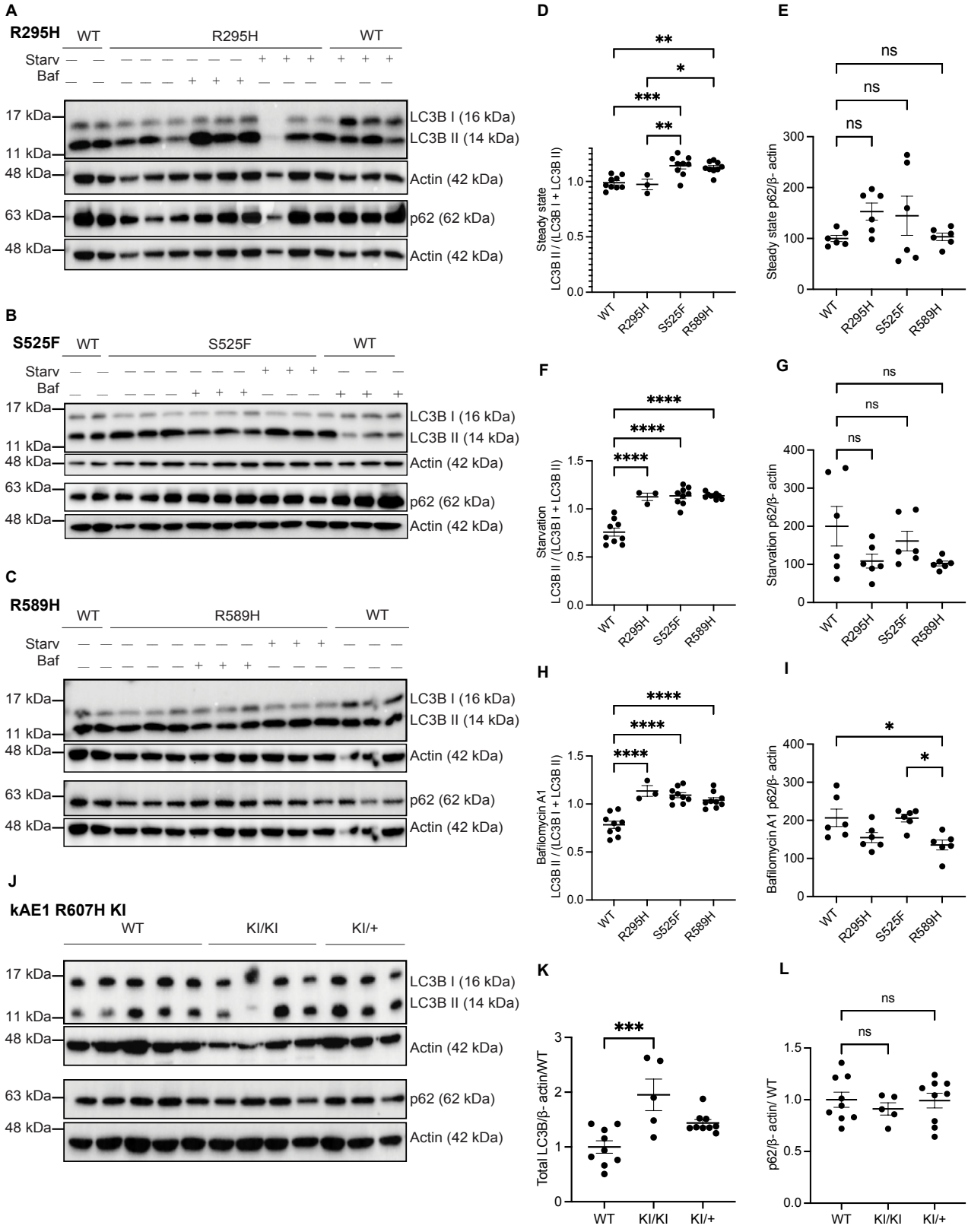

Figure 2 Essuman et al.

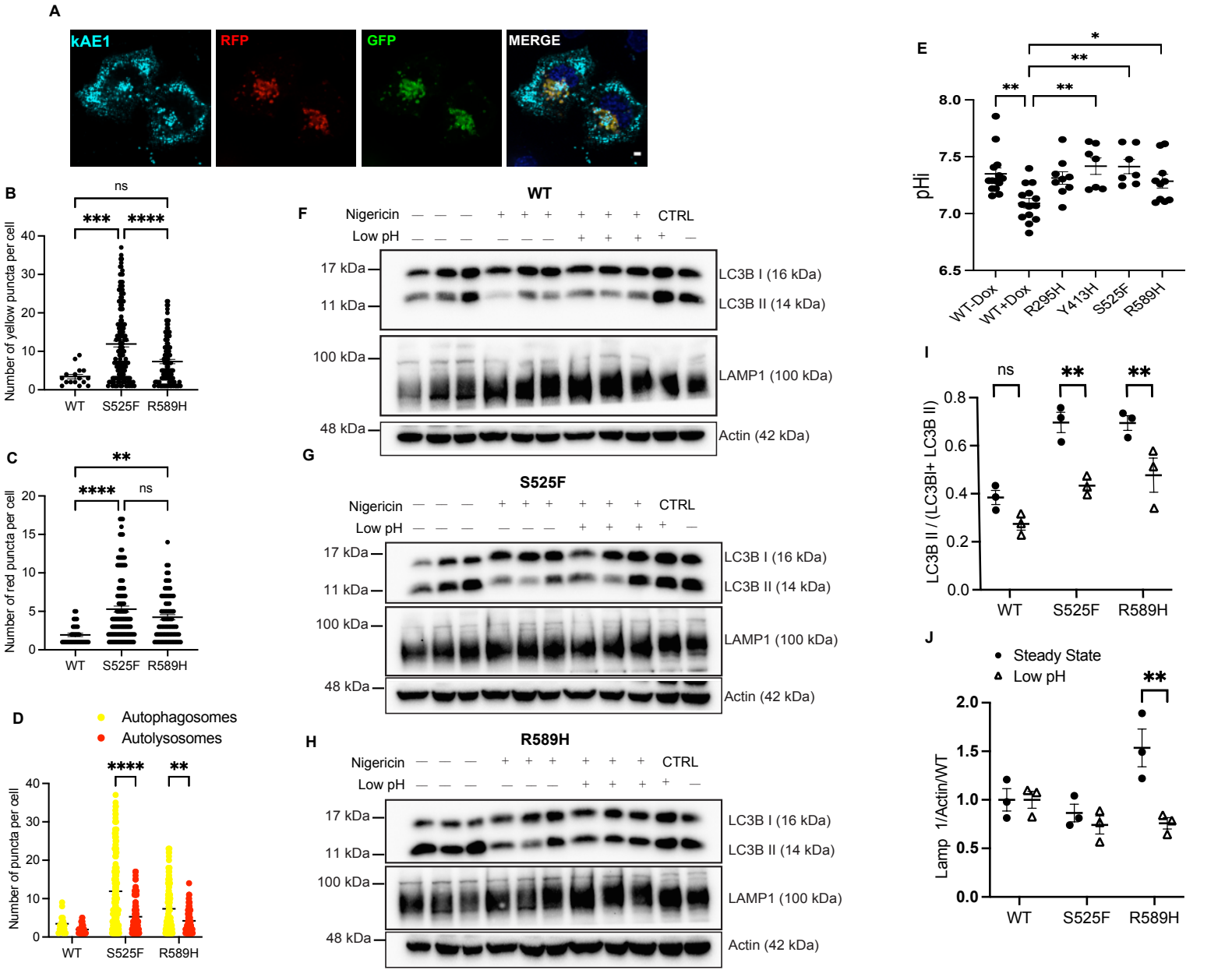

Figure 3 Essuman et al.

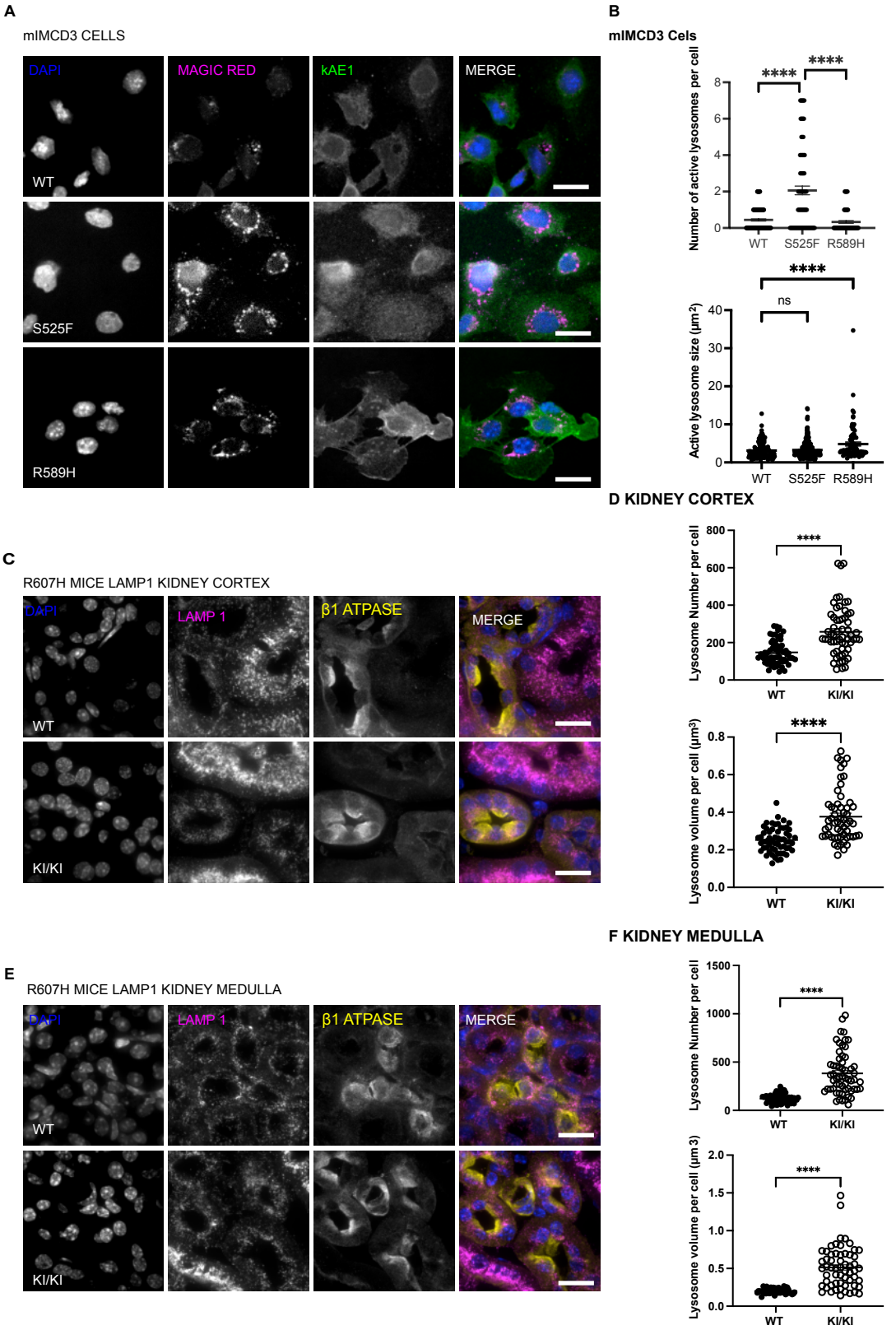

Figure 4 Essuman et al.

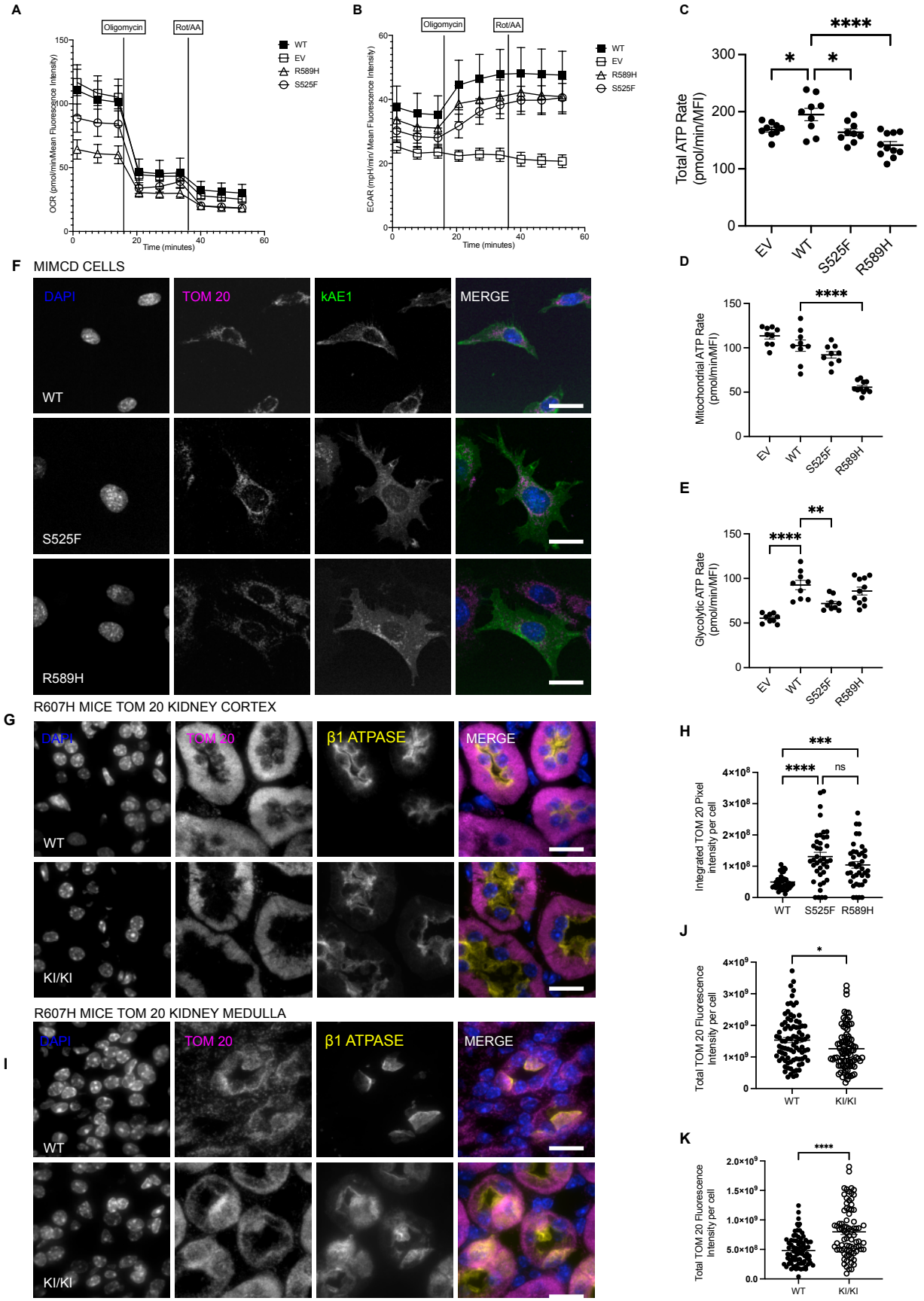

Figure 5 Essuman et al.